GEOPHYSICS, VOL. 66, NO. 1 (JANUARY-FEBRUARY 2001); P. 137–147, 15 FIGS.

Mapping of induced polarization using natural fields

Erika Gasperikova and H. Frank Morrison*

ABSTRACT

The observed electromagnetic response of a finite body is caused by induction and polarization currents in the body and by the distortion of the induction currents in the surrounding medium. At a sufficiently low frequency, there is negligible induction and the measured response is that of the body distorting the background currents just as it would distort a direct current (dc). Because this dc response is not inherently frequency dependent, any observed change in response of the body for frequencies low enough to be in this dc limit must result from frequency-dependent conductivity. Profiles of low-frequency natural electric (telluric) fields have spatial anomalies over finite bodies of fixed conductivity that are independent of frequency and have no associated phase anomaly. If the body is polarizable, the electric field profile over the body becomes frequency dependent and phase shifted with respect to a reference field.

The technique was tested on data acquired in a standard continuous profiling magnetotelluric (MT) survey over a strong induced polarization (IP) anomaly previously mapped with a conventional pole-dipole IP survey. The extracted IP response appears in both the apparent resistivity and the normalized electric field profiles.

INTRODUCTION

The standard field technique for mapping IP relies on the use of grounded electrodes, most commonly in the dipole-dipole or pole-dipole configuration. A current is introduced into the ground through two current electrodes, and potential difference is measured between two potential electrodes located at some distance from the current electrodes. In the frequency domain, the apparent resistivity, or the impedance phase, is measured at frequencies low enough that any electromagnetic (EM) coupling is either negligible or predictable. EM coupling increases with the receiving dipole length and dipole separation and with conductivity and frequency (Dey and Morrison, 1973). For deep exploration, the dipoles and their separation must be large; hence, the operational frequency must be low to avoid EM coupling. Unfortunately, the natural EM field spectrum rises steeply below 1.0 Hz. Achieving an adequate signal-to-noise ratio therefore requires excessive power or costly attempts to reduce contact resistance at the current electrodes. Even for exploration at shallow depths, the need to inject current reduces the usefulness of the technique in many situations in which it is difficult to achieve low contact resistances.

There has been great interest in making IP measurements by using EM methods (Hohmann et al., 1970; Flis et al., 1989), and especially in using natural EM fields for this purpose. EM methods can achieve greater depth of penetration with geometrically smaller configurations than resistivity arrays, and because they need not contact the ground, surface resistivity is not a factor. Furthermore, there is the tantalizing possibility that the IP effect might be measured with an airborne system. The use of natural fields is particularly attractive for deep exploration because the problems alluded to above for standard IP surveys would be avoided. The increasing natural field spectrum, that is, noise in the traditional IP surveys, would become the desirable signal source in a natural field method. At the John S. Sumner Memorial International Workshop on Induced Polarization, held at the University of Arizona in October 1994, the general topic of measuring IP with EM methods was assigned a high priority for future research and development (Ward et al., 1995).

Flis et al. (1989) demonstrated the conditions under which the IP phenomenon could be observed in time-domain EM (TEM) surveys. Basically, the observed response from a conducting polarizable body is caused by induction currents in the body, the distortion of induction currents in the surrounding medium, and polarization currents. In the absence of induction currents, the polarization currents are governed by dc relationships. In the time domain, all currents are present in varying degrees, but if the decay rate of the polarization currents is lower than the decay rate of the induced currents, then the polarization currents dominate at some time, the observed magnetic

Manuscript received by the Editor November 9, 1998; revised manuscript received May 12, 2000.
*University of California at Berkeley, Engineering Geoscience, 1 Cyclotron Road, MS 90-1116, Berkeley, California 94720. Email: erika.gasperikova@alum.calberkeley.org; hfmengeo@socrates.berkeley.edu.

fields can reverse in sign, and the IP effect therefore can be recognized.

A more basic statement is that if the EM response of a body in the ground is in the dc limit, then the IP effect is separable from the induction response. This simply means that at some frequency, no induction in the body occurs; the external response is that of the body distorting the background currents just as it would distort a dc current. Because this dc response is not inherently frequency dependent, any observed change in response of the body for frequencies low enough to be in this dc limit must result from frequency-dependent conductivity. The difficulty that must be anticipated in implementing this concept is that the size and conductivity of the target must be identified first so as to distinguish changes in its response from the continuum of the EM induction response from the surrounding medium. Target dimension and conductivity information are important for calculating a skin depth that helps to define a frequency range and profile length necessary for recovering IP response from the data.

Ware (1974) first recognized that the process of conductor identification and consequent separation of IP and inductive responses might be simplest for natural field plane-wave sources such as those used for magnetotellurics (MT). He found that for the mode in which the electric field (E) is perpendicular to strike, now called the TM mode, the response of a simple 2-D body indeed reached a dc limit at some frequency, f_c, below which the change in EM response was negligible. Thus, any observed changes in the electric profile for frequencies below f_c would be caused by the intrinsic resistivity change of the body. Ware concluded that for models representing typical exploration targets, the IP response will predominate over the EM induction response for frequencies of 0.1 Hz and lower. He did several numerical simulations using realistic frequency-dependent resistivities and showed that the effect should be measurable. In a field experiment, however, he discovered that the resolution of the measurement equipment at that time was not sufficient for the task.

MODEL STUDY

To illustrate asymptotic dc behavior, we have simulated the MT response for a 2-D model shown in Figure 1. The 10 ohm-m block is a rectangular prism, 100 m × 100 m in a cross-section located in a half-space of 100 ohm-m. The depth to its top is 30 m. The TM apparent resistivity (ρ_a) cross-section for a bandwidth of 0.001 Hz to 100 Hz is shown in Figure 2a. This response clearly shows what is called the static limit; below about 1.0 Hz, the section becomes invariant with frequency. It also should be noted that the phase shown in Figure 2b becomes essentially constant for frequencies below about 0.1 Hz. The actual value of the phase is dictated by the volume of the background medium wherein induction is present. For this model, the phase asymptotes to the uniform half-space value of −135°. If the body shown in Figure 1 had a frequency-dependent resistivity for frequencies at which the inductive response was negligible (in which the apparent resistivity and phase have reached the static dc limit), then the profiles of the electric fields at two such frequencies would reveal the IP response of the body.

The MT forward models used in this simulation were run by using the numerical algorithm developed by Wannamaker et al. (1987), which was modified to include a frequency-dependent conductivity for any region within the discretization mesh. The resistivity was specified by a generalized Cole-Cole

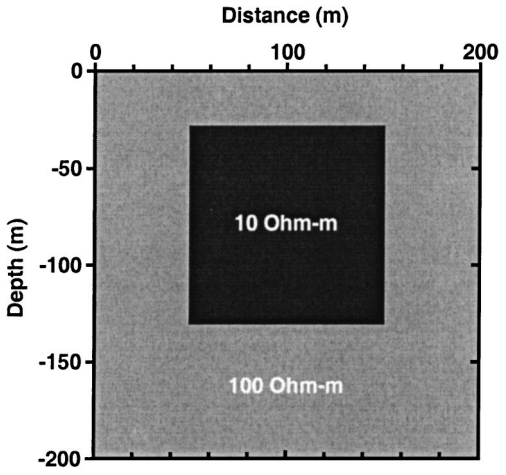

FIG. 1. Two-dimensional model of a 10 ohm-m block, 100 × 100 m, at a depth of 30 m in a 100 ohm-m half-space.

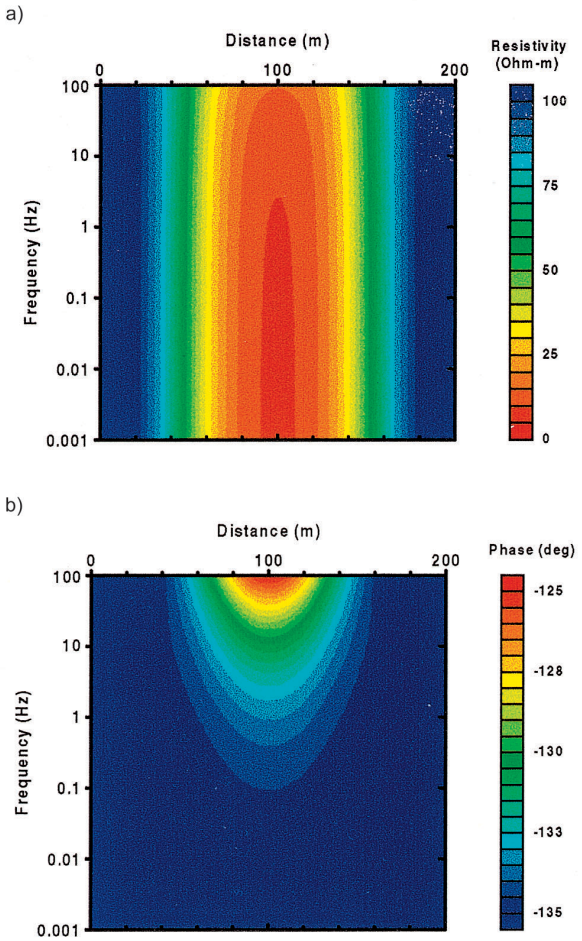

FIG. 2. (a) Apparent resistivity cross-section for the TM mode for the model of Figure 1. (b) Phase cross-section for the TM mode for the model of Figure 1.

representation (Pelton, 1977)

$$\rho(\omega) = \rho_0\left[1 - m\left(1 - \frac{1}{(1 + (i\omega\tau)^c)^a}\right)\right] \qquad (1)$$

with ρ_0 the low-frequency resistivity asymptote, m the chargeability, and τ the time constant. The exponents a and c control the frequency dependence. If exponent c is equal to 1, this becomes a Cole-Davidson representation.

In this study, the parameters were chosen to replicate the frequency dependence reported by Van Voorhis et al. (1973). They used an empirical mathematical model called the Drake model, which is a special case of the Cole-Davidson representation for $m = 1$. The values of target resistivity and phase used in the block model of Figure 1 are shown in Figure 3. Parameters used for this calculation are $\rho_0 = 10$ ohm-m, $m = 1$, $\tau = 318.3$, $c = 1$, and $a = 0.0969$. The response was calculated for the frequency range of 0.0001 to 10 Hz. Van Voorhis et al. (1973) define the percent frequency effect (PFE) as

$$\mathrm{PFE} = 100\frac{\rho(\omega) - \rho(A\omega)}{\rho(\omega)} \qquad (2)$$

$$\mathrm{PFE} = 100(1 - A^{-a}) \qquad (3)$$

where the constant A specifies the spread between measurement frequencies. The above parameters produce a 20% PFE.

Profiles of apparent resistivity and phase at 0.01 and 0.1 Hz are shown in Figures 4a and 4b, respectively, and a profile of the percent frequency effect (PFE) calculated from the curves at those frequencies is shown in Figure 4c. The apparent PFE over the target is 16%. For this model, the phase anomalies are less than 3°, but probably are detectable in good-quality data.

The above modeling example is oversimplified because there are no competing frequency-dependent effects from adjacent bodies or structures. Such effects, in practice, might make it difficult to separate the frequency dependence seen over the target body. The model shown in Figure 5 is representative of a more complex geology encountered in the field experiment described below. A highly chargeable thermal contact zone is located on the flank of a porphyry intrusive surrounded by marine sediments. The surrounding near-surface sediments are unconsolidated valley fills, and these overlie a more resistive basement. In the highly schematic model of Figure 5, the polarizable body has a dc resistivity of 5 ohm-m. It is displaced from the major porphyry intrusive (100 ohm-m) and is in a host

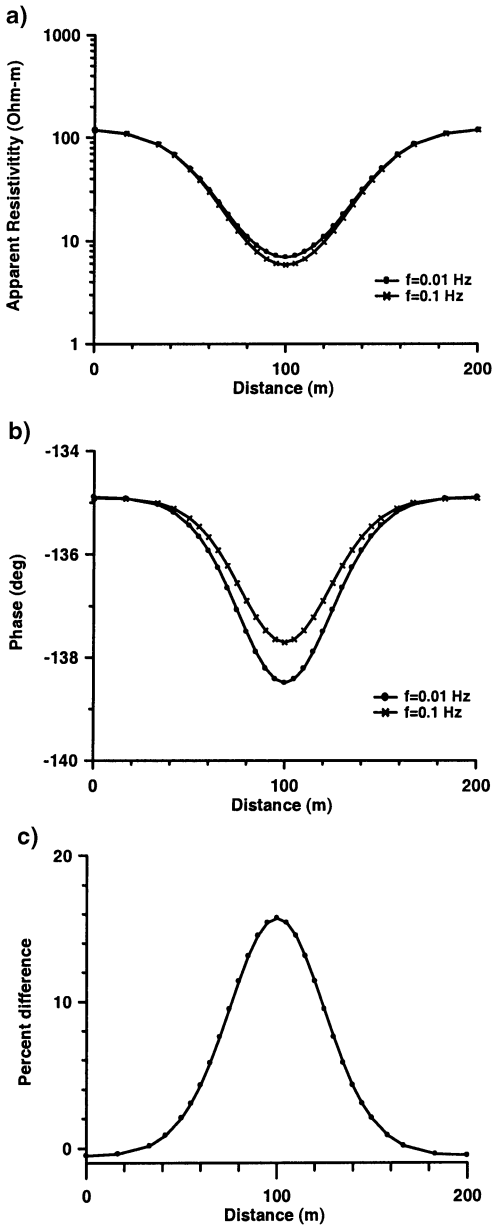

FIG. 4. (a) Profiles of apparent resistivity at 0.01 and 0.1 Hz for the model of Figure 1. (b) Profiles of phase at 0.01 and 0.1 Hz for the model of Figure 1. (c) Percent difference between the apparent resistivity profiles at 0.01 and 0.1 Hz for the model of Figure 1.

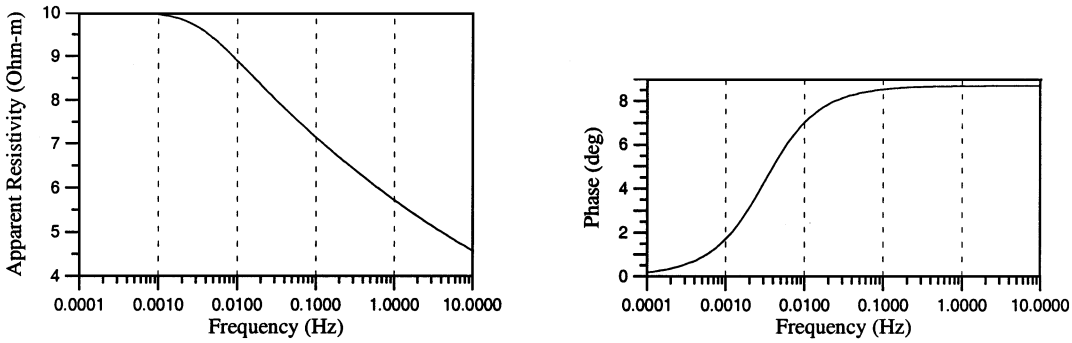

FIG. 3. The generalized Cole-Cole apparent resistivity and phase-versus-frequency dependence for the target block in Figure 1.

medium of 20 ohm-m. At the extreme right of the section lies a conductive nonpolarizable (5 ohm-m) section of valley-fill sediments. For this model, a 20% intrinsic PFE has been used. The parameters m, τ, a, and c used in this calculation had the same values as in the previous model.

The profiles of apparent resistivity and phase at frequencies of 0.1 and 0.01 Hz are shown in Figures 6a and 6b. The phase anomaly in the field data from a conventional pole-dipole survey over the target conductor is about 50 milliradian (mrad), or 2.8°, which compares to an intrinsic value of 3.5° at 0.01 Hz. In this model, strong variations occur in the apparent resistivity, caused by the conductive sediments on the right and the resistive intrusive on the left of the target zone. The apparent resistivity and phase profiles reflect the large-scale variations in the inductive response determined mainly by the lateral contrast between the intrusive and the sediments. This is particularly evident in the phase plots for 0.01 and 0.1 Hz, which progressively depart from the half-space value of −135° to −146° at 0.1 Hz. Similarly, the apparent resistivities asymptote to different values for each frequency over the uniform layered structures at the ends of the model. No deep large-scale structure is incorporated into the model, and the 100 ohm-m medium essentially becomes a background medium for the whole profile at the depth of 4400 m. Hence, both ends of the profile are in the static dc limit for frequencies below 0.1 Hz, and the change of resistivity with frequency, $d\rho/df$, is the same at both ends of the profile.

Note that if one wants to use phase for detection of the IP effect, it should be done in two steps. First, the large-scale variations in the inductive response (regional trend) should be identified. Second, small changes (i.e., a few degrees) from that background value coinciding with the spatial extent of the anomalous body should be found.

To observe the IP effect, the resistivity profiles must be shifted in the ordinate direction, because their ratios in the dc limit must be one. In Figure 6c, the profiles at 0.1 and 0.01 Hz have been shifted vertically to coincide over the right and left ends of the section (where it is clear that the dc limit has been achieved). Although the profiles themselves are much more complex than those for the single target block (Figures 2a and 2b), the separation in apparent resistivity that occurs between stations 2000 and 3000 is very clear. This separation, expressed as a percent difference between the 0.1 and 0.01 Hz profiles, is shown in Figure 6d on an expanded scale. The maximum difference is more than 15% over the target.

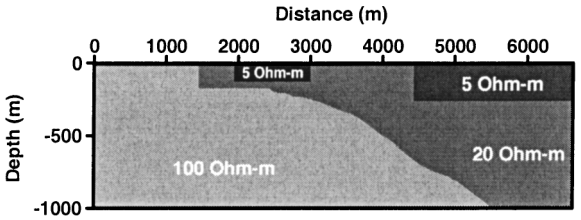

FIG. 5. Two-dimensional resistivity model representative of the geologic cross-section of the field survey site.

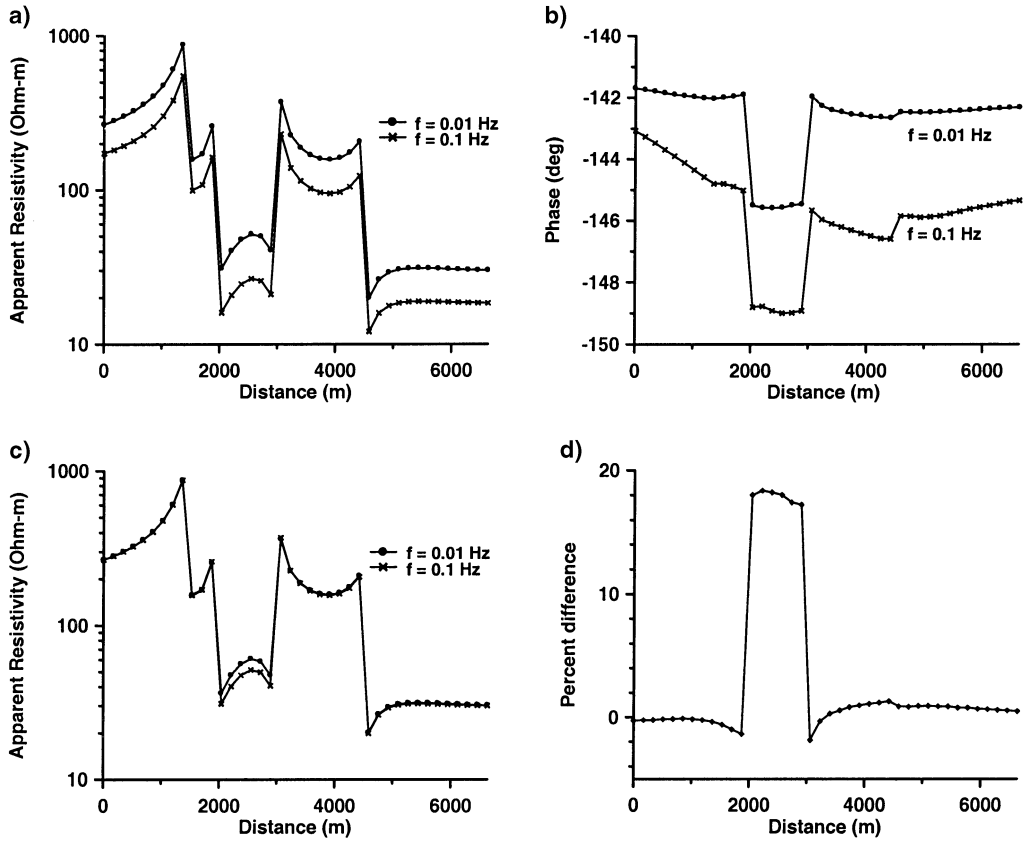

FIG. 6. (a) Profiles of apparent resistivity at 0.01 and 0.1 Hz for the model of Figure 5. (b) Profiles of phase at 0.01 and 0.1 Hz for the model of Figure 5. (c) Profiles of apparent resistivity at 0.01 and 0.1 Hz for the model of Figure 5, vertically shifted to coincide on the right and left ends of the profile. (d) Percent difference between the apparent resistivity profiles at 0.01 and 0.1 Hz for the model of Figure 5 after having been shifted.

We have described the IP effect in terms of the apparent resistivity used in MT. This approach increases the resistivity anomalies because the apparent resistivity varies with the square of the electric field. In the next section, we describe a method of extracting the IP effect by using profiles of the electric fields themselves.

EXTRACTION OF THE IP RESPONSE

In the telluric method, the electric field measured by a traversing dipole is normalized by the field at a fixed or reference dipole on the line. This transfer function depends on relative changes in the conductivity beneath the traversing dipole. As we saw in the previous model studies, this transfer function becomes frequency independent when the conductivity structure beneath the traversing dipole is in the dc limit. Any observed frequency dependence at low frequencies is indicative of IP.

The telluric method has been used mainly as a low-cost method for determining the structure of sedimentary basins, with most of the pioneering work in this field done in France, Germany, and the former Soviet Union. After a few attempts to test the applicability of the telluric method in geothermal areas (e.g., Beyer, 1977), it was concluded that the conductivity anomalies did not lend themselves to quantitative interpretation (Goldstein, 1988). Slankis et al. (1972) reported 8 Hz telluric measurements made in the vicinity of heavy sulfide deposits. Relative resistivity measurements, obtained by comparison of telluric amplitudes, revealed the location of conductive sulfide bodies, provided that width was greater than depth of burial. Possible detection of IP was not considered. Ware (1974) also suggested that natural telluric field variations should be monitored simultaneously at a "reference" dipole recording site and at a succession of dipoles that traverses an area of interest, to extract the IP effect. In this study, we have used the models described in the previous section to illustrate means of extracting IP from telluric profiles.

In the TM mode, the magnetic field (H) is constant, so changes in apparent resistivity over the body are caused solely by changes in electric field (E) measured across the structure. Profiles of real and imaginary parts of the electric field at 0.01 Hz for the body of Figure 1, with and without IP, are shown in Figure 7a. Without the IP effect, the real and imaginary parts are identical. (The phase, with respect to the magnetic field, is set by the background medium, which in this case is a half-space. The phase of the reference electric field is consequently -135°.) For the frequency dependence we have chosen, the change in the imaginary part as a result of the IP effect is much more significant than the change in the real part. If the reference-site electric field is $Ae^{i(\omega t+\varphi_1)}$ and the electric field along the profile is $Be^{i(\omega t+\varphi_2)}$, then the ratio between these two fields can be expressed as $\frac{B}{A}\cos(\varphi_2-\varphi_1)+i\frac{B}{A}\sin(\varphi_2-\varphi_1)$. If the structure is in the static dc limit and no IP is present, there is no phase shift between these two electric fields and thus no imaginary component in the ratio. However, if the dipole along the profile traverses a body with IP, $(\varphi_2-\varphi_1)$ is nonzero, and therefore an imaginary component exists. The advantage of using the imaginary part of the ratio is that it is easier to see small changes with respect to zero than to look for the changes with respect to some background number of unknown amplitude. Therefore, the electric field along the profile normalized by the electric field at a site without IP, the reference site, can reveal the position of the IP target. Figure 7b shows the imaginary part of the normalized electric field for the body of Figure 1. The imaginary part of the normalized electric field below 1.0 Hz clearly identifies the position of the IP structure.

The same procedure was applied to the model of Figure 5. Profiles of the real and imaginary parts of the electric field at 0.01 Hz for the structure, with and without IP, are shown in Figure 8a. Both components coincide over the area without IP, while there is a significant difference in the response between stations 2000 and 3000 where the IP structure is located. Figure 8b shows a cross-section of the imaginary part of the normalized electric field for the same model. As before, the normalization is done with the electric field values at the right extreme of the section. The lightly shaded "dike," extending below 0.1 Hz between stations 2000 and 3000, clearly identifies the position of the IP structure.

The lateral resolution of a feature displaying an IP effect is quite good, but there is little vertical resolution. Only if the polarization can be logically (geologically) associated with a conductivity contrast (as in the case of the Figure 1 body) can the vertical bounds and intrinsic IP effect be determined.

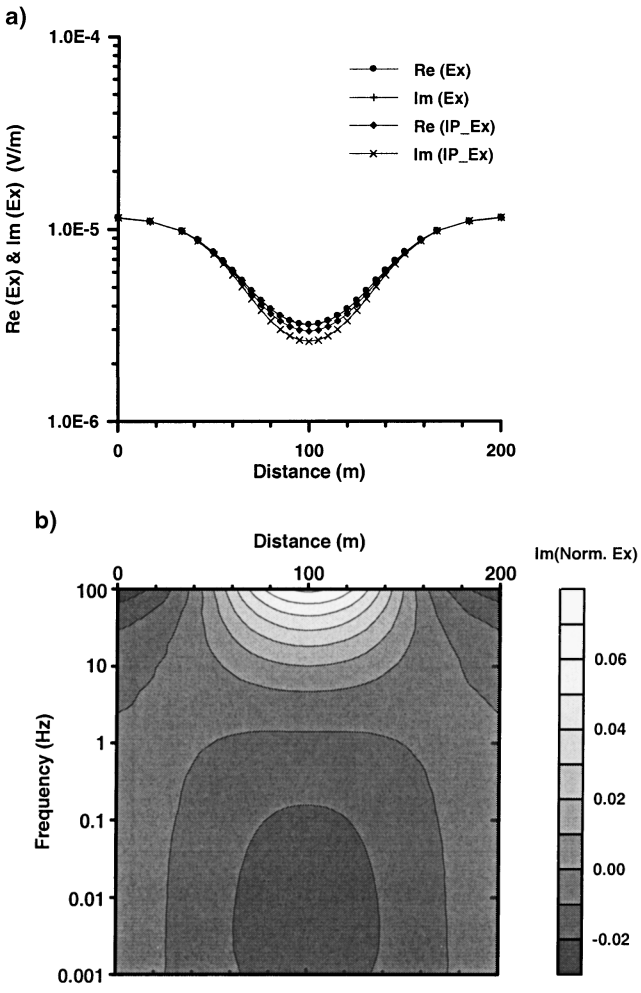

FIG. 7. (a) Profiles of the real and imaginary parts of the electric field at 0.01 Hz for the model of Figure 1. (b) Cross-section of the imaginary part of the normalized electric field for the model of Figure 1 with IP.

The above procedure requires the knowledge from the conductivity cross-section of which features are in the dc limit and therefore are candidates for detection by the imaginary part of the transfer function.

FIELD EXPERIMENT

Data from two MT field surveys on the same mineral prospect near Battle Mountain, Nevada, were analyzed to detect a possible IP effect. A schematic geologic cross-section for this area, shown in Figure 9, and the results of a pole-dipole IP/resistivity survey, shown in Figure 10, were provided by Western Mining. No vertical scale appears in Figure 9 because it is only a conceptual model. However, the ratio between vertical and horizontal scale in the plot might be considered to be about 2 (Gary Oppliger, 1995, personal communication). The pole-dipole IP/resistivity survey was done with a dipole length of 200 m, with the transmitter on the right side of the receiver. dc and IP inversions of the pole-dipole data were done by using the DCIP2D algorithm by Oldenburg and Li (1994). The resistivity inversion (Figure 10c) recovers a highly conductive structure at the right extreme of the profile, which represents valley sediments, and a very resistive structure on the left of station 4500, the contact with the porphyry. A small, near-surface conductive structure is located right on the edge of the porphyry, between stations 4500 and 5000, which may represent the thermal contact zone. The IP inversion (Figure 10d) honoring the near-surface phase data shows that a zone of high chargeability lies between stations 4300 and 4800, straddling the contact. A large-scale feature extends at depth between stations 3500 and 4500.

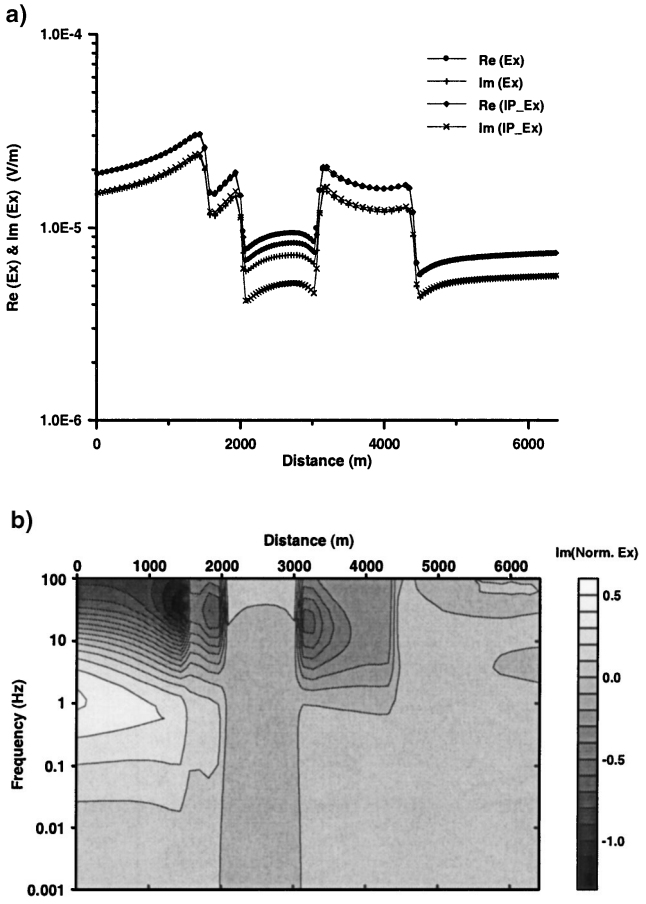

FIG. 8. (a) Profiles of the real and imaginary parts of the electric field at 0.01 Hz for the model of Figure 5. (b) Cross-section of the imaginary part of the normalized electric field for the model of Figure 5.

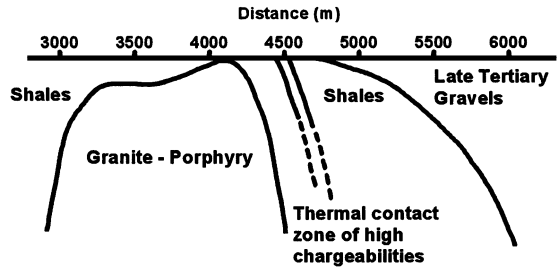

FIG. 9. Schematic geologic cross-section of the Battle Mountain profile (courtesy of Western Mining).

The MT survey was laid out along a line of the previous IP/resistivity survey. Two MT surveys were conducted along this profile. In the 1995 survey, a complete data set of orthogonal electric field (E) profiles was acquired. The MT survey was conducted under standard commercial survey specifications, with excellent data in the 0.1 to 300 Hz band. Data were recorded in remote reference mode, where the remote site consisted of both orthogonal electric and magnetic sensors. Along the profile, data were taken in segments consisting of two pairs of contiguous orthogonal electric dipoles with one pair of orthogonal magnetic sensors. Acquisition time was about one hour per setup.

From a geologic mapping perspective, this survey was very successful. The TM mode apparent resistivity and the impedance phase are shown in Figure 11. The MT section clearly shows the contact with the porphyry at 4500 m and reveals the adjoining small conductor in the vicinity of stations 4700 to 5000, as well as a section of horizontal conductor from 5000 m to the end of the profile. The skew of the tensor impedance (Figure 11c) shows strong three-dimensionality for frequencies below 0.05 Hz in the vicinity of the porphyry. This strongly suggests that 2-D inversion of any electrical data in this vicinity may be in error.

The TM data were inverted with the RRI algorithm of Smith and Booker (1991), and the resulting section, Figure 11d, is in excellent agreement with the pole-dipole inversion shown in Figure 10c. The electrical and MT data refine the geologic sketch by locating the contact. The impedance strike was nearly orthogonal to the line; rotation had essentially no impact on the analysis of the TM mode data.

Unfortunately, the data quality between 0.01 and 0.1 Hz was not accurate enough to yield a profile of relative low-frequency E phase and amplitude response over the whole profile. An objective demonstration of the IP effect thus could not be achieved. However, by careful data selection, very accurate apparent resistivities at frequencies of 0.01 and 0.1 Hz were obtained on eight continuous dipoles in the midportion of the profile. The apparent resistivity values at 0.1 and 0.01 Hz are plotted in Figure 12a. The porphyry contact is seen clearly at station 4500 as it is in the resistivity pseudosection

(Figure 10a). This data further refines the schematic of Figure 9.

There are not enough data points along this profile to derive systematic electric field ratios for a band of frequencies across the whole profile. In this situation, we can draw only on our previous knowledge of the geology and attempt to see if there is an effect where we know it is. It is known from the IP/resistivity survey that the section to the right of station 5000 is conductive, has little IP phase, and is over the valley-fill sediments. If we assume that there are no IP effects in the MT data to the right of station 5000, then we simply can shift one of the profiles in Figure 12a so that it overlies the other profile to the right of 5000 m. This result is shown in Figure 12b, where it is seen that the data overlay is exact on the right-hand portion of the line, but the profiles are displaced between 4300 m and 4700 m. The higher-frequency (0.1 Hz) apparent resistivities are about 15% less than the lower-frequency (0.01 Hz) values. This anomaly is centered directly over the resistivity and IP phase anomaly that lies beneath 4500 m. The MT data in these two profiles have inherent errors of about 5%. Thus, the split in the values for these two frequencies is defined well and appears to reflect the known IP effect at this site.

A second survey was conducted along the same profile in May 1996. The new survey was designed with several features to improve the overall quality of the data. The first consideration was to increase significantly the data-recording time to improve the accuracy of the data at low frequencies. A far remote site (consisting of both orthogonal magnetic and electric sensors) located a few kilometers away and a near remote site (consisting of both orthogonal magnetic and electric sensors) at the beginning of the profile were used for reference. To get high-quality data at low frequencies, data acquisition time was 6–12 hours per setup.

With standard processing, there were still only selected frequencies for which accurate data were available. Profiles of apparent resistivity at frequencies 0.1 and 0.01 Hz are plotted in Figure 13a. The same procedure that was applied to 1995 data was applied to this data set. Assuming no IP effects in the MT data to the right of station 5000, we simply can shift one of the profiles in Figure 13a so that it overlies the other profile to the right of 5000; this result is shown in Figure 13b. Again, as in Figure 12b, the data overlay is exact on the right-hand portion of the line, but to the left of 5000, the profiles are displaced. The resulting percent difference curve is shown in Figure 13c. The dashed line in Figure 13c represents a regional trend in the data, resulting from large-scale structures. Because we are interested only in smaller-scale structures, any significant positive departure from this trend is caused by the IP body. Negative values in the percent difference plot suggest that the left side of the profile is still in the EM regime. The higher-frequency (0.1 Hz) apparent resistivities between stations 4200 and 4800 are about 15% less than the lower-frequency (0.01 Hz) values. The IP effect is resolved better than in the previous survey, and the IP zone is defined well between stations 4200 and 4800—precisely over the high chargeability seen in the IP-phase pseudosection (Figure 10b). The MT data in these two profiles have inherent errors less than 5%, with the split in the values for these two frequencies well defined. Expressing the differences as a

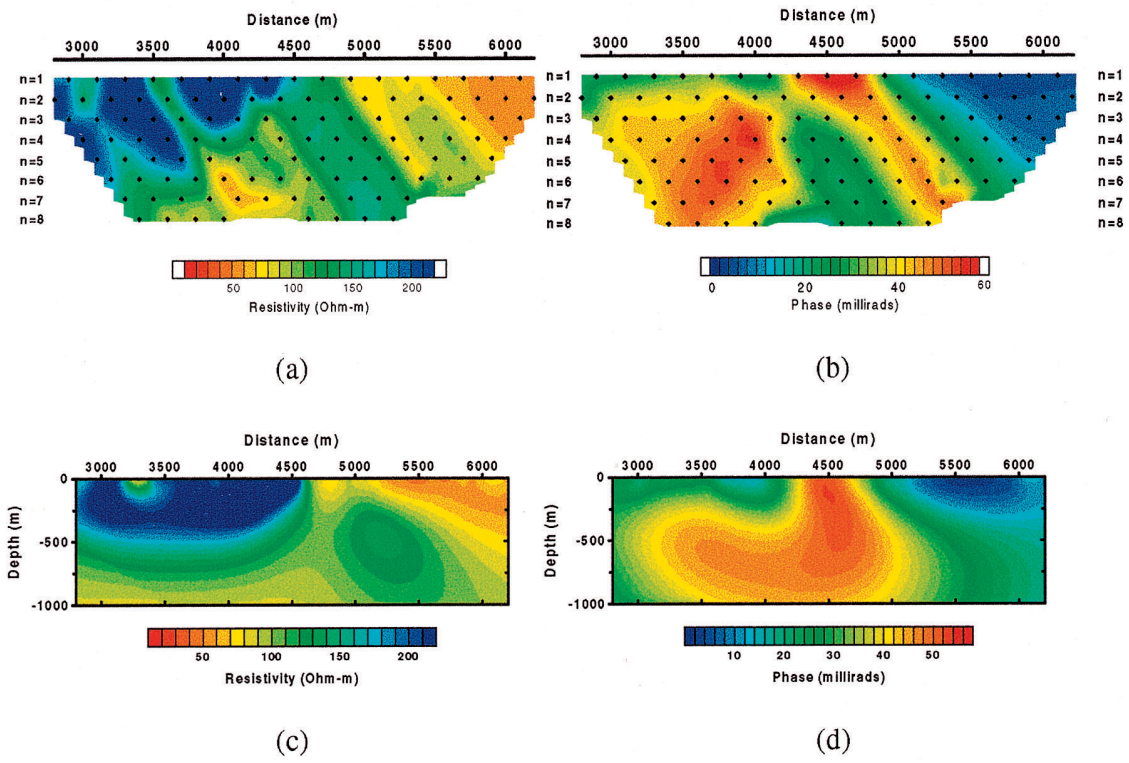

FIG. 10. (a) Pole-dipole resistivity pseudosection, (b) IP phase pseudosection, (both courtesy of Western Mining); (c) resistivity inversion of pole-dipole data, (d) phase inversion of pole-dipole data.

percent of one of the apparent resistivities removes the influence of the background resistivity and, in this case, shows that the inherent PFE is approximately the same in the zone on either side of the contact.

We next attempted to improve the results by using a new, robust multichannel spectral-analysis code (Egbert, 1997). This code uses a robust estimation procedure to reduce unwanted noise (outliers), but more importantly, it uses all channels at all the sites to compute interstation transfer functions and tensor magnetotelluric impedances at each station. Because we worked with high-quality data, no significant difference arose between the magnetotelluric impedance estimations and subsequent apparent resistivity calculations using this program and the standard processing technique. However, in working only with electric fields, which for this survey had a higher signal-to-noise ratio than the magnetics, we obtained excellent estimates of the electric field transfer function down to about 0.01 Hz. We then displayed results in the normalized electric field, as described above.

Figure 14a shows a cross-section of the imaginary part of the normalized electric field along the MT profile. The data points have inherent errors of about 2%. Therefore, any variation larger than 2% can be an indication of the IP target. The lightly shaded area between stations 4500 and 5200 and the darker area between stations 4000 and 4500, both centered at about 0.04 Hz, clearly show the IP effect that coincides with IP anomalies known from the IP/resistivity survey. A profile of the imaginary part of the normalized electric field at 0.04 Hz is shown in Figure 14b. Unlike the crude single-frequency difference plot of Figures 12 and 13, the results of the normalized field analysis display the coherence of the IP response over a broad band of frequencies and in a well-defined zone of the profile. The imaginary part of the normalized fields preserves the intrinsic resistivity information: The contact is clearly seen in the middle of the anomaly. This field data analysis suggests a contact model with IP on either side.

To confirm these observations, we constructed the model shown in Figure 15a. Here, a contact zone within a porphyry, as well as an adjacent conductive zone, is assigned intrinsic IP following the same Cole-Davidson model as used previously. Figure 15b shows a cross-section of the imaginary part of the normalized electric field for this model. Again, the resistive body has a strong IP effect (about −0.15), while the IP effect of the conductive body is about −0.03.

After the first field survey, we learned that to improve the accuracy of the data at low frequencies, we must increase the data recording time significantly. Because the cost-effectiveness of the survey is a concern, we have tried to determine the minimum time required in field acquisition to detect or define the IP response. Our analysis suggests that an acquisition time of two hours at each station should be sufficient for good data quality between 0.1 and 0.01 Hz. If the anomaly is weak, four hours of recording time might be necessary.

CONCLUSIONS

Clearly, as shown in the model study and two surveys over the same target, the IP effect can be recovered from MT profiling data.

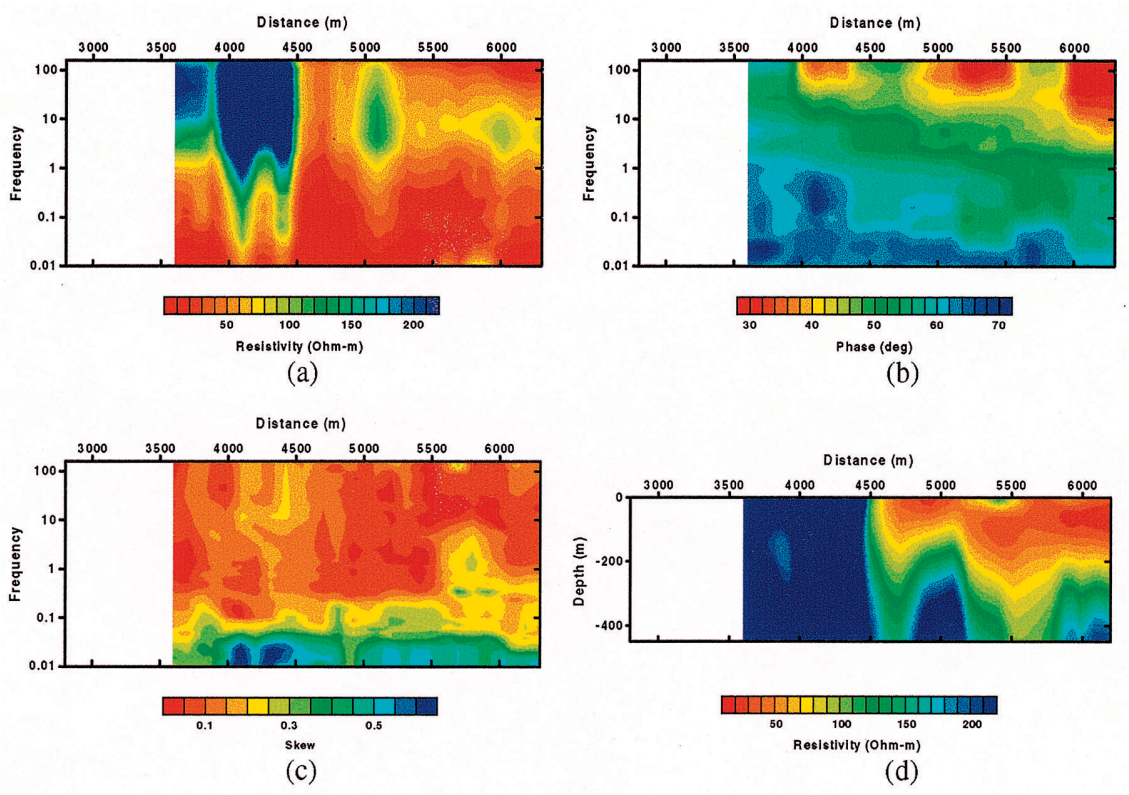

FIG. 11. (a) Raw TM apparent resistivity cross-section, (b) raw TM phase cross-section, (c) skew of tensor impedance cross-section, (d) RRI inversion of TM data along MT profile.

The classic telluric profiling technique, wherein the complex ratio of the profiling electric dipole and fixed reference dipole is plotted as a function of frequency and profile position, is a simple and robust procedure for recovering the effect. We obtained the desired accuracy using the robust multichannel spectral analysis of Egbert (1997).

In summary, the following four conditions must be realized to detect the IP effect:

1) The IP effect must be confined to a finite body. The method cannot work in layered earth or in 2-D earth for the TE mode (E parallel to strike). In both these cases, there is no dc limit—induction is always present and the frequency-dependent conductivity cannot be separated from the frequency-dependent EM response.
2) The intrinsic IP effect, the change in conductivity with frequency, must be present for those frequencies below those causing induction in the body.
3) The field data must be rotated to yield the electric field normal to the strike. In a true 2-D situation, this rotation yields E/H values for the TM mode. For this mode, H is constant along the profile, so either ρ_a ($\sim|E|^2$) or E can be used to infer the presence of IP.
4) The MT data must be of sufficient precision that the changes in E and its phase are, in fact, detectable.

The required data quality is obtained easily with modern MT equipment. Our analysis suggests that with the multichannel spectral analysis code of Egbert (1997), an acquisition time

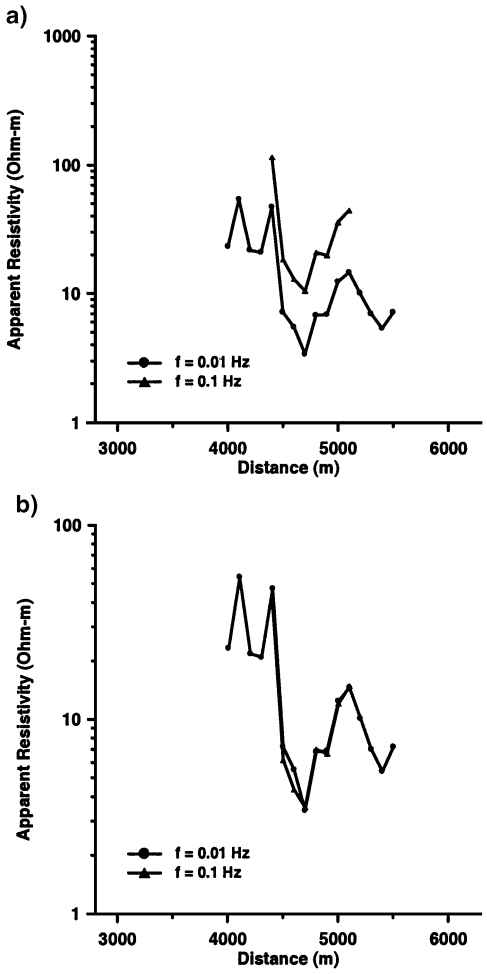

FIG. 12. (a) Profiles of apparent resistivity at 0.01 and 0.1 Hz from 1995 MT survey. (b) Profiles of apparent resistivity at 0.01 and 0.1 Hz from 1995 MT survey, shifted to coincide at the right-hand extreme of the profile.

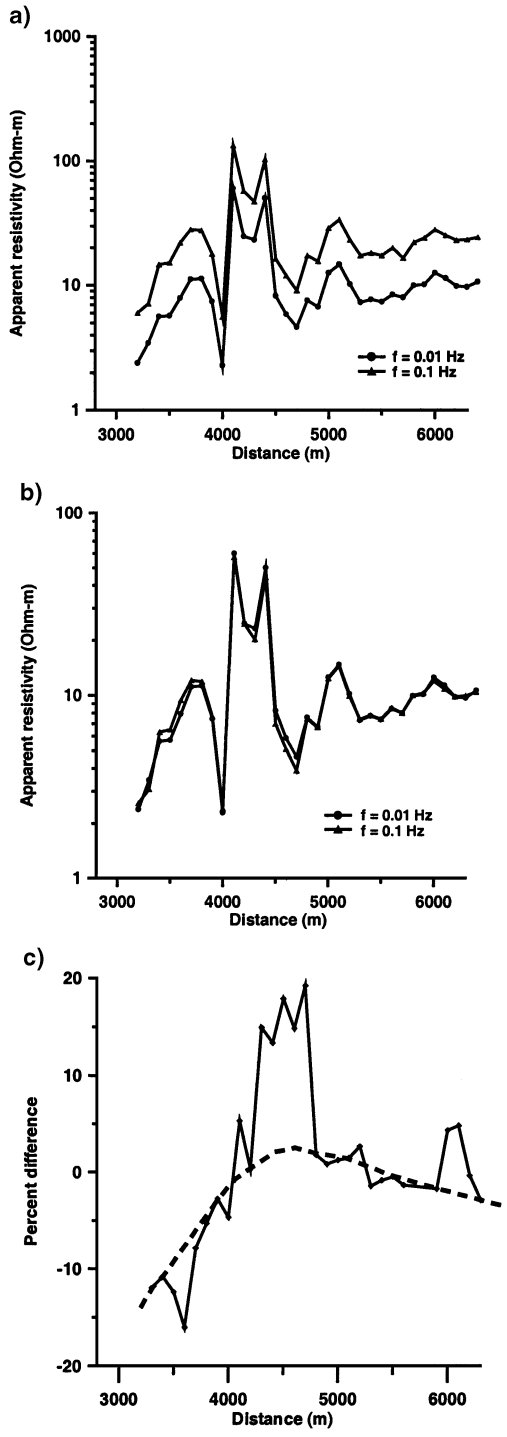

FIG. 13. (a) Profiles of apparent resistivity at 0.01 and 0.1 Hz. (b) Profiles of apparent resistivity at 0.01 and 0.1 Hz, shifted to overlap on the right-hand portion of the profile. (c) Percent difference between the apparent resistivity profiles at 0.01 and 0.1 Hz, after having been shifted.

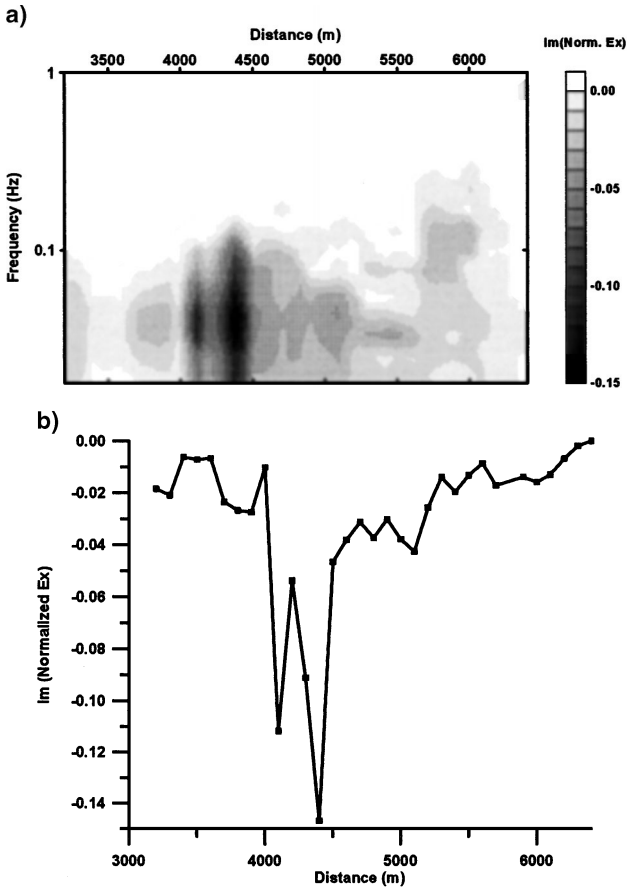

FIG. 14. (a) Cross-section of the imaginary part of the normalized electric field. (b) Profile of the imaginary part of the normalized electric field at 0.04 Hz.

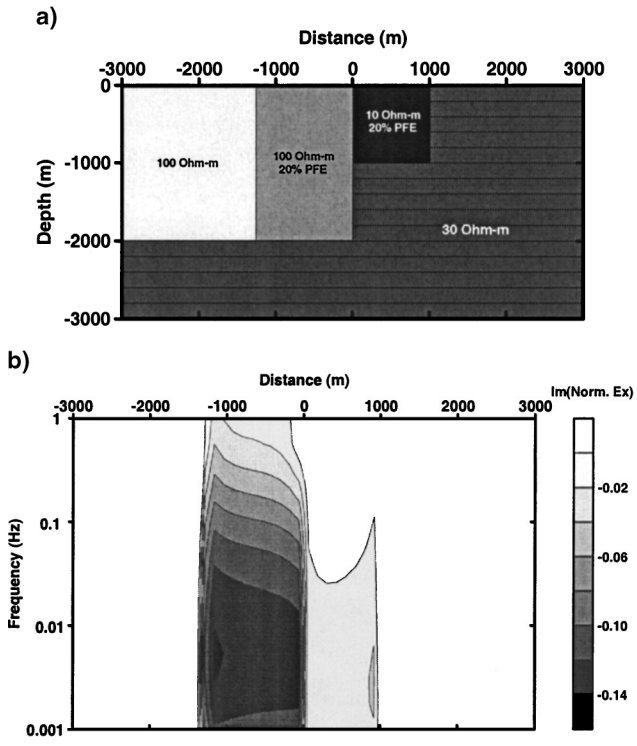

FIG. 15. (a) Model of resistive and conductive body with IP. (b) Cross-section of the imaginary part of the normalized electric field.

of two hours should be sufficient for good data quality between 0.1 and 0.01 Hz. However, if the anomaly is weak, four hours of recording time might be necessary. With new 24-bit technology and with more than 10 channels acquired at a time, detecting IP using natural EM fields (natural field IP, or NFIP) could became cost-effective for the identification of IP targets. The NFIP cost per line-kilometer is similar to the current commercial rate (about $2000/km) for production IP/resistivity surveys. The advantage of the NFIP survey is that it eliminates logistical difficulties with transmitter deployment in the field and inherently provides a greater depth of exploration than conventional IP/resistivity surveys. In addition, valuable information about the strike and dimensionality of the subsurface can be obtained from the tensor impedances.

Although the method was illustrated using shallow targets, the same procedure can be used for an identification of deeper structures. As long as the ratio between the size of the body and skin depth stays the same, the magnitude of the response should not change. However, it may be observable only at lower frequencies, depending on when the structure reaches its static dc limit and if an IP response still exists at those low frequencies, as in condition (2) in the list above.

This analysis could be taken into three dimension as 3-D modeling algorithms become available. The finite size of the body makes a 3-D target a strong candidate for this kind of analysis because at some frequency, the body should reach its dc limit in any profile direction. Separation of the IP response from the EM response thus should be easier than for the 2-D bodies assumed in this study.

ACKNOWLEDGMENTS

This work has been sponsored by Aberfoyle Resources Ltd., BHP Minerals, Codelco, CRA Exploration, EMI Inc., Geodatos S.A.I.C., Homestake Mining, INCO Exploration, Kennecott, MIM Exploration, Newmont Exploration Ltd., Placer Dome Inc., and Western Mining Exploration S.A. We thank the Geophysical Inversion Facility at the University of British Columbia for providing DCIP2D software, and D. Oldenburg, D. Alumbaugh, and two anonymous reviewers for reviewing this manuscript and for their helpful suggestions.

REFERENCES

Beyer, J. H., 1977, Telluric and dc resistivity techniques applied to the geophysical investigations of Basin and Range geothermal systems: Ph.D. thesis, Univ. of California at Berkeley.

Dey, A., and Morrison, H. F., 1973, Electromagnetic coupling in frequency and time-domain induced-polarization surveys over a multilayered earth: Geophysics, **38**, 380–405.

Egbert, G. D., 1997, Robust multiple-station magnetotelluric data processing: Geophys. J. Internat., **130**, 475–496.

Flis, M. F., Newman, G. A., and Hohmann, G. W., 1989, Induced polarization effects in time domain electromagnetic measurements: Geophysics, **54**, 514–523.

Goldstein, N. E., 1988, Subregional and detailed exploration for geothermal-hydrothermal resources, Geother. Sci. & Tech., **1**, 303–431.

Hohmann, G. W., Kintzinger, P. R., Van Voorhis, G. D., and Ward, S. H., 1970, Evaluation of the measurement of induced electrical polarization with an inductive system: Geophysics, **35**, 901–915.

Oldenburg, D. W., and Li, Y., 1994, Inversion of induced polarization data: Geophysics, **59**, 1327–1341.

Pelton, W. H., 1977, Interpretation of induced polarization and resistivity data: Ph.D. thesis, Univ. of Utah, Salt Lake City.
Slankis, J. A., Telford, W. M., and Becker, A., 1972, 8 Hz telluric and magnetotelluric prospecting: Geophysics, **37**, 862–878.
Smith, J. T., and Booker, J. R., 1991, Rapid inversion of two- and three-dimensional magnetotelluric data: J. Geophys. Res., **96**, 3905–3922.
Van Voorhis, G. D., Nelson, P. H., and Drake, T. L., 1973, Complex resistivity spectra of porphyry copper mineralization: Geophysics, **38**, 49–60.
Wannamaker, P. E., Stodt, J. A., and Rijo, L., 1987, A stable finite-element solution for two-dimensional magnetotelluric modeling: Geophys. J. Roy. Astr. Soc., **88**, 277–296.
Ward, S. H., Sternberg, B. K., LaBrecque, D. J., and Poulton, M. M., 1995, Recommendations for IP research, The Leading Edge, **14**, 243–247.
Ware, George Hunter, 1974, Theoretical and field investigations of telluric currents and induced polarization: Ph.D. thesis, Univ. of California at Berkeley.